

Wave-Function Mapping of Graphene Quantum Dots with Soft Confinement

D. Subramaniam,¹ F. Libisch,² Y. Li,³ C. Pauly,¹ V. Geringer,¹ R. Reiter,² T. Mashoff,¹ M. Liebmann,¹ J. Burgdörfer,² C. Busse,⁴ T. Michely,⁴ R. Mazzarello,³ M. Pratzer,^{1,*} and M. Morgenstern¹

¹*II. Physikalisches Institut B and JARA-FIT, RWTH Aachen University, D-52074 Aachen, Germany*

²*Institute for Theoretical Physics, Vienna University of Technology, A-1040 Vienna, Austria*

³*Institute for Theoretical Solid State Physics and JARA-FIT, RWTH Aachen University, D-52074 Aachen, Germany*

⁴*II. Physikalisches Institut, Universität zu Köln, Zùlpicherstrasse 77, D-50937 Köln, Germany*

(Received 19 April 2011; published 23 January 2012)

Using low-temperature scanning tunneling spectroscopy, we map the local density of states of graphene quantum dots supported on Ir(111). Because of a band gap in the projected Ir band structure around the graphene K point, the electronic properties of the QDs are dominantly graphenelike. Indeed, we compare the results favorably with tight binding calculations on the honeycomb lattice based on parameters derived from density functional theory. We find that the interaction with the substrate near the edge of the island gradually opens a gap in the Dirac cone, which implies soft-wall confinement. Interestingly, this confinement results in highly symmetric wave functions. Further influences of the substrate are given by the known moiré potential and a 10% penetration of an Ir surface resonance into the graphene layer.

DOI: 10.1103/PhysRevLett.108.046801

PACS numbers: 73.20.At, 72.10.Fk, 73.21.Fg, 73.22.Pr

Graphene has moved in short time from first preparation as a small flake [1] towards possible applications such as high frequency transistors [2], supercapacitors [3], or touch screens [4]. Another exciting perspective is to use graphene quantum dots (QDs) as spin qubits [5]. The basic prerequisite is a very long spin-coherence time [6], which might exist in graphene [7] due to the absence of hyperfine coupling in isotopically pure material and the small spin-orbit coupling [8]. First graphene QDs have been produced and probed by transport measurements [9,10]. However, since graphene provides no natural gap, it is difficult to control the electron number [11]. Moreover, the 2D sublattice symmetry makes the QD properties very susceptible to the atomic edge configuration [5] unlike conventional QDs. As a result, chaotic Dirac billiards have been predicted [12] and were even claimed to be realized [9,13]; i.e., the wave functions are assumed to be rather disordered. To achieve improved control of graphene QDs, the QD edges must be well defined and a deeper understanding of the QD properties is mandatory.

Direct insight into QD properties is provided by scanning tunneling spectroscopy (STS) which maps out the squared wave functions of QDs [14] and, at the same time, determines the shape of the QD atom by atom. Using STS, we probe graphene QDs with well-defined zigzag edges supported on an Ir(111) surface [15]. These QDs maintain graphene properties as the filled part of the graphene Dirac cone lies in the Ir projected band gap [16]. By comparing the measured wave functions with model calculations, we determine the relationship between geometry and electronic properties and extract general trends. Most notably, the soft edge potential provided by the interaction of the QD edges with the substrate enhances the geometrical symmetry of the wave functions, thus

rendering the QD more regular. The susceptibility of the wave functions to the edge configuration is intimately related to the additional sublattice symmetry (pseudospin) which makes graphene so special [17]. Also the moiré pattern induced by the graphene-Ir lattice mismatch [16] and the hybridization of graphene with an Ir surface resonance are shown to have an influence on the measured wave functions.

STM measurements are performed in ultrahigh vacuum at $T = 5$ K [18]. Monolayer graphene islands are prepared by exposing clean Ir(111) for 4 min to a pressure of 10^{-5} Pa of C_2H_4 at 300 K and subsequent annealing to 1320 K (30 s) [19]. The resulting graphene QDs have diameters of 2–40 nm as shown in Fig. 1(a). Atomically resolved QD images [Figs. 1(b) and 1(c)] reveal the complete enclosure of the QDs by zigzag edges.

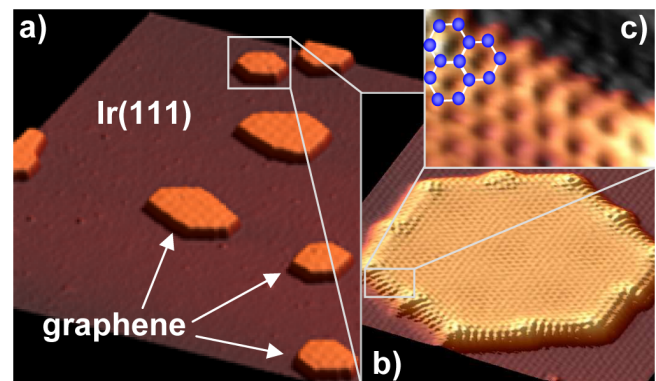


FIG. 1 (color online). (a) (100×100) nm² STM image of Ir(111) covered by monolayer graphene islands; $U = -0.3$ V, $I = 0.3$ nA; (b) atomically resolved (12×12) nm² image of graphene island; (c) magnified view of zigzag edge with graphene lattice overlaid; $U = 0.7$ V, $I = 20$ nA.

The local density of states (LDOS) of 15 islands is mapped by STS. We use a lock-in technique with modulation frequency $\nu = 1.4$ kHz and amplitude $U_{\text{mod}} = 10$ mV resulting in an energy resolution $\delta E \approx \sqrt{(3.3k_B T)^2 + (1.8eU_{\text{mod}})^2} = 18$ meV [20]. For dI/dU curves, we stabilize the tip at sample voltage U_{stab} and current I_{stab} . Figure 2(a) shows a dI/dU curve laterally averaged over the hexagonal QD shown to the right. It displays three maxima below the Dirac point E_D , which is slightly above the Fermi level E_F [16]. Thus, the peaks belong to confined hole states. Figures. 2(b)–2(d) show dI/dU maps at the peak energies. For the first peak ($U = -0.26$ V), one maximum of the LDOS in the center of the island appears, a ring shaped structure is observed at $U = -0.42$ V, and, a maximum-minimum-maximum sequence from the center towards the rim with an additional star-shaped angular dependence is visible at $U = -0.63$ V. We checked that no other LDOS shapes are present at -1.4 eV $\leq U \leq 0$ V. From the sequence of observed

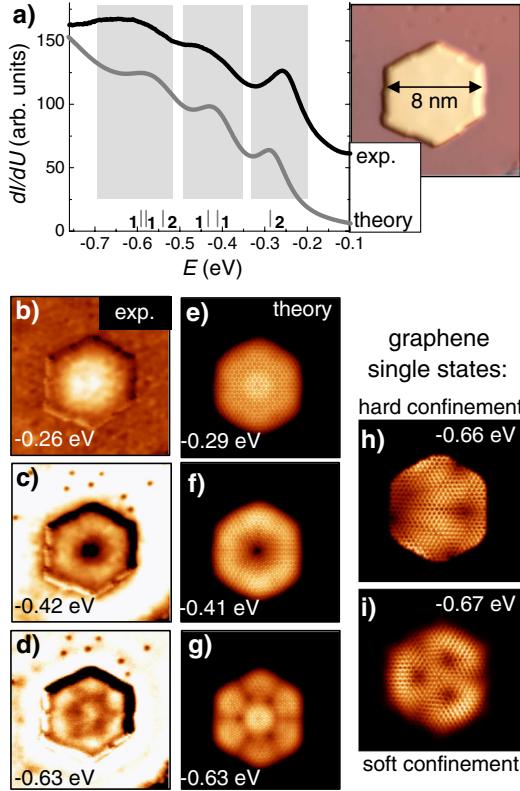


FIG. 2 (color online). (a) black line: $dI/dU(U)$ curve spatially averaged over the graphene QD shown to the right; $U_{\text{stab}} = 0.5$ V, $I_{\text{stab}} = 0.5$ nA, $U_{\text{mod}} = 10$ mV; gray line: DOS(E) of the same island as obtained by TB calculation (see text); vertical bars mark the calculated eigenstate energies with degeneracies indicated as numbers; (b)–(d) dI/dU images recorded at energies $E = Ue$ as marked; $I = 0.2$ nA; $U_{\text{mod}} = 10$ mV. (e)–(g) LDOS maps calculated with soft edge potential at energies indicated; (h),(i): LDOS of an individual state calculated without (h) and with (i) soft edge potential.

LDOS shapes we conclude that they represent confined states of the QD.

To model the QD states, we employ third-nearest neighbor tight binding (TB) calculations [21–23] using the atomic configuration of the QD found by STM,

$$H = \sum_{i,s} |\phi_{i,s}\rangle V_i \langle \phi_{i,s}| + \sum_{(i,j),s} \gamma_{(i,j)} |\phi_{i,s}\rangle \langle \phi_{j,s}| + \text{H.c.} \quad (1)$$

The $\gamma_{(i,j)}$ are hopping amplitudes between sites i and j being $\gamma_{(i,j)} = (3.14, 0.042, 0.35)$ eV for the (first, second, third) nearest-neighbors [21]. The V_i represent local on-site potentials.

We first employed a spatially constant V_i within the islands, i.e., hard-wall-confinement. Regular, but also very irregular wave functions result, as shown in Fig. 2(h) and Figs. 3(e)–3(g). The irregular wave functions often display a large intensity at the rim of the QDs and illustrate the sensitivity of graphene QDs to details of the edge configuration [5,12]. Such irregular shapes, however, were never found in the present STS experiments featuring about 50 different states [24].

This failure is related to the two experimental facts that (i) a graphene flake bends downward from $D = 3.4$ Å in the center of a QD to $D = 1.6$ Å at its rim [15,25] and that (ii) the entire graphene flake features a moiré type corrugation leading to minigaps [16,26,27].

To incorporate effect (i) we determined the band structure of graphene by *ab initio* density functional theory

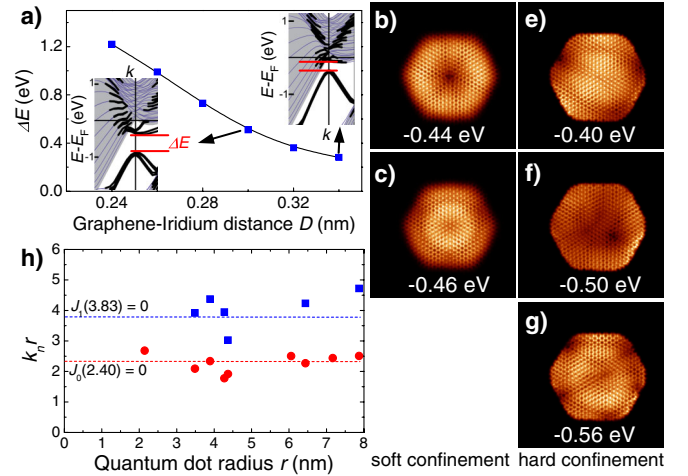


FIG. 3 (color online). (a) Energy gap ΔE versus graphene-Ir distance D as deduced from DFT calculations; insets: band structure around E_D for two different D as marked by arrows with ΔE indicated; grey area: projected bulk bands of Ir; Thick black lines: graphene states; (b)–(g) Calculated LDOS ($= |\Psi|^2$) for individual confined states with energies marked: (b)–(d) with soft edge potential; (e)–(g) without soft edge potential; (h) experimental $k_n r = E_n / (\hbar v_D) r$ for the two peaks closest to E_D at different average island radius r ; circles: $n = 0$, squares: $n = 1$; dotted lines: zeros of the first two Bessel functions (see text).

(DFT) calculations [24,28] for different graphene-Ir surface distances D . Upper and lower limits for D were set by the known distance between extended graphene layers and Ir(111), $D = 3.4 \text{ \AA}$ [25] and the smallest distance found at the edge of a graphene island, $D = 1.6 \text{ \AA}$ [15]. A proper description of Ir(111) surface states requires thick slabs which makes it unfeasible to use the large 10×10 supercell necessary to account for the graphene-Ir lattice mismatch. Therefore, a slightly compressed Ir lattice is used making graphene and Ir(111) commensurate. This allows us to work with a slab of 24 Ir layers with graphene on both sides and a vacuum space of 20 \AA between slabs. The insets in Fig. 3(a) exhibit the resulting band structures for two different fixed D . The size of the gap ΔE is plotted in Fig. 3(a). We incorporate the effect of the D dependent band gap on V_i within the TB through [12]:

$$V_{i,\text{rim}} = \Delta E[D(r_i)]/2\sigma_z, \quad (2)$$

where the Pauli matrix σ_z acts on the sublattice degree of freedom. A homogeneous $V_{i,\text{rim}}$ would open a gap of size ΔE at E_D . The functional form of $\Delta E[D] = (0.7 \times (3.6 - D[\text{\AA}])^2 + 0.23) \text{ eV}$ is taken from the fit to the DFT calculations [Fig. 3(a)]. We model the global height variation of a graphene QD by linear increase of $D(r)$ from the rim towards 10 \AA inside the island as suggested by the DFT calculations of [15]. We checked that reasonable modifications do not change the results significantly [24].

To incorporate effect (ii), we added a moiré potential $V_{i,m}$ to V_i . Based on the experimentally observed minigap of 200 meV [16,26,27], we use a harmonic variation of $V_{i,m}$ in each of the three dense packed directions of graphene with a total amplitude of 400 meV [24]. Finally, the peak width Γ of the eigenstates is adapted to the experiment leading to $\Gamma(E) = 0.33|E|$.

The resulting LDOS curve [gray line, Fig. 2(a)] as well as the calculated LDOS maps [Figs. 2(e)–2(g)] exhibit excellent agreement with the experimental data. Importantly, the calculations yield only states that reflect the hexagonal symmetry of the QD shape in agreement with experiment, but none of the irregular states found without smooth confinement [24]. This can be rationalized by the suppressed interaction of the confined states with the zigzag edges, which would break sublattice symmetry [29]. The increased geometrical symmetry is illustrated in Figs. 3(b)–3(g) comparing wave functions of the same quantum dot with soft (hard) confinement leading to symmetric (irregular) states. Thus, softly opening a band gap at the QD edge leads to strongly improved control on the states residing in its interior. To illustrate this crucial finding, we show that the state energies in our QDs can be correctly estimated by a simplified circular flake geometry. We obtain $E_n = \hbar v_D k_n$ with Dirac velocity $v_D = 10^6 \text{ m/s}$ and k_n deduced from the zeros of the zeroth and first Bessel function:

$$J_n(k_n r) = 0, \quad n = 0, 1. \quad (3)$$

Up to an island area of $A = 150 \text{ nm}^2$ (average radius: $r = \sqrt{A/\pi}$), the estimate fits the experimental peak energies to within $\sim 20\%$ for the two lowest energy states [Fig. 3(h)]. Larger islands do not follow this trend because of their strong deviation from a circular shape [e.g., Fig. 4(a)]. Obviously, neither the sensitive sublattice symmetry of graphene [5], nor the influence of the iridium substrate enter Eq. (3) showing the simplicity of softly confined graphene QDs.

In larger islands, we observe the influence of $V_{i,m}$ on wave-function patterns directly, at energies $E < -0.6 \text{ eV}$. Figure 4(a) shows an STM topography of a large QD exhibiting a regular moiré pattern [19]. The dI/dU map in Fig. 4(b) and the calculated LDOS in Fig. 4(c) reproduce the moiré topography albeit with inverted amplitude. The

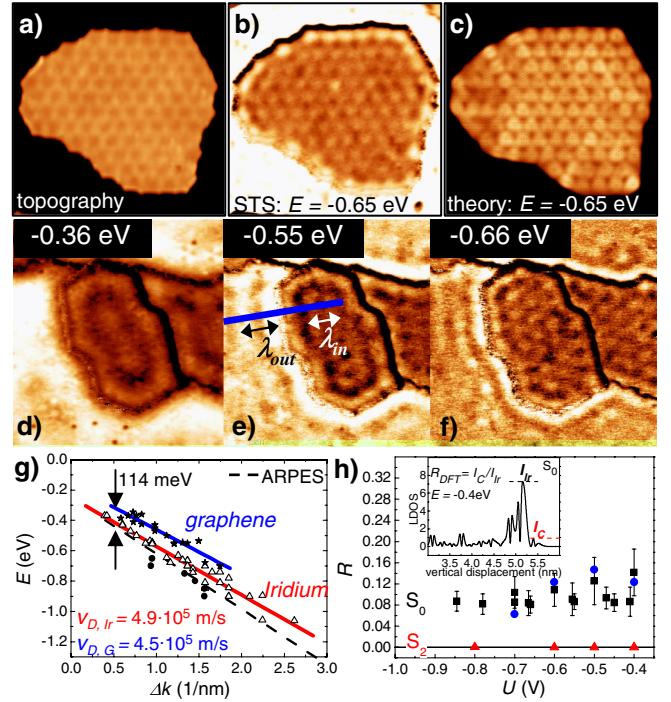


FIG. 4 (color online). (a) STM image and (b) dI/dU map of a large graphene QD; $30 \times 30 \text{ nm}^2$, $U = -0.65 \text{ V}$, $I = 0.5 \text{ nA}$, $U_{\text{mod}} = 10 \text{ mV}$; (c) calculated LDOS of the same QD at $E = -0.65 \text{ eV}$; (d)–(f) dI/dU maps of a graphene QD recorded at the energies marked; $27 \times 30 \text{ nm}^2$, $I = 0.5 \text{ nA}$, $U_{\text{mod}} = 10 \text{ mV}$; deduced wave lengths λ_{out} (λ_{in}) outside (inside) the QD are marked in (e); (g) resulting dispersion relations $E(\Delta k = \pi/\lambda_{\text{in/out}})$ inside (stars) and outside (triangles) of the QD as well as from standing waves scattered at Ir(111) step edges (circles); full lines are linear fits with resulting v_D indicated; energy offset is marked; dashed line is deduced from photoemission on clean Ir(111) [27]; (h) relative intensity R of S_0 and S_2 in graphene as deduced from STS data (squares) and from DFT calculations (S_0 : circles, S_2 : triangles); inset: calculated LDOS of S_0 at $E = -0.4 \text{ eV}$ along the direction perpendicular to the surface; I_{Ir} and I_{C} as used for determination of R are marked.

same result is found for all larger islands [24]. We checked that normalizing the dI/dU images to account for a spatially varying tip-surface distance [30] did not change the LDOS patterns.

One feature, already visible by comparing Figs. 4(b) and 4(c), is not accounted for by a spatially varying V_i : a bright rim of the island in the dI/dU image. This rim is found for all islands, but cannot be reproduced by the TB calculations [24]. Closer to E_D , this feature develops into a standing wave pattern that finds its counterpart outside the island with slightly larger wave length λ [Figs. 4(d)–4(f)]. The dispersion relations $E(\Delta k = \pi/\lambda)$ [31] inside and outside the islands are evaluated as displayed in Fig. 4(e) and in [24] for 11 islands. They are shown together with results from standing waves at step edges of Ir(111) in Fig. 4(g). The $E(\Delta k)$ curves are linear according to $E = -\hbar v_D \Delta k + E_D$ with $v_D \approx 4.9 \times 10^5$ m/s, $E_D = -0.3$ eV outside the island and $v_D \approx 4.5 \times 10^5$ m/s, $E_D = -0.2$ eV inside the island. These values agree with those of the Ir surface resonance S_0 around $\bar{\Gamma}$ found by photoemission (dashed line) including the energy offset between the two $E(\Delta k)$ curves [27]. The values disagree with v_D for the graphene Dirac cone on Ir(111) by a factor of 2 and with E_D for the Ir S_2 surface state by 0.5 eV [16]. Thus, the standing wave patterns within the QD are attributed to an intrusion of S_0 into graphene.

The amplitude of the standing wave in the islands A_G is found to be close to the amplitude outside the island A_{Ir} for several islands and energies [24]. This is surprising considering the fact that the tip is 0.23 nm further away from the Ir surface, when positioned above graphene, which would suggest a reduction in dI/dU intensity by a factor of 100 [20]. However, DFT calculations reveal that S_0 , exhibiting sp symmetry, penetrates into graphene. The ratio between the LDOS in the graphene layer I_C and the LDOS in the Ir surface layer I_{Ir} is $R_{DFT} = I_C/I_{Ir} \approx 8 - 12\%$ [inset of Fig. 4(h)]. For comparison, S_2 shows only $R_{DFT} \approx 0.02\%$. Figure 4(h) favorably compares R_{DFT} of S_0 with the data from STS R_{STS} where the apparent A_G/A_{Ir} is rescaled according to $R_{STS} = A_G/A_{Ir} e^{\alpha \delta}$ [20] with $\alpha = 1.1 - 1.2/\text{\AA}$ deduced from $I(z)$ curves and $\delta = 1.1 \text{\AA}$ being the difference between real height (3.4 \text{\AA} [25]) and apparent STM height (2.3 \text{\AA}) of the graphene above the Ir(111). Thus, we can quantitatively reproduce the strength of S_0 intrusion into graphene. A simple explanation for the strong S_0 intrusion is not obvious, but we note that, according to DFT, also the d_z^2 -like surface state S_1 , located at E_F and exhibiting no dispersion [16], penetrates into graphene with $R \approx 10 - 40\%$ and the π electrons of graphene penetrate back into Ir with $R \approx 1 - 4\%$.

In conclusion, we mapped the LDOS of graphene QDs supported on Ir(111). For small islands, properties of an isolated graphene QD with soft edge potential reproduce the measured wave functions. Most importantly, the soft

edge induced by the substrate is required for the experimentally observed high symmetry of the wave functions. Larger islands show an additional standing wave pattern caused by an intruding Ir surface resonance and signatures of the moiré potential.

We acknowledge helpful discussions with N. Atodiresei, C. Stampfer, G. Burkard, S. Runte, and a referee, as well as financial support by DFG (LI 1050/2-1, MO 858/8-2, BU 2197/2-1), Fonds National de la Recherche (Luxembourg), and FWF (SFB-F41 VICOM). Numerical calculations are performed on the Vienna Scientific Cluster (VSC).

Note added in proof.—During the referee process, two publications with similar experimental results have been published [32], which were submitted later than our manuscript.

*pratzer@physik.rwth-aachen.de

- [1] K. S. Novoselov *et al.*, *Science* **306**, 666 (2004).
- [2] Y. M. Lin *et al.*, *Science* **332**, 1294 (2011); **327**, 662 (2010); Y. Q. Wu *et al.*, *Nature (London)* **472**, 74 (2011).
- [3] Y. Zhu *et al.*, *Science* **332**, 1537 (2011).
- [4] K. S. Kim *et al.*, *Nature (London)* **457**, 706 (2009).
- [5] B. Trauzettel *et al.*, *Nature Phys.* **3**, 192 (2007); S. Das Sarma *et al.*, *Rev. Mod. Phys.* **83**, 407 (2011).
- [6] D. Loss and D. P. DiVincenzo, *Phys. Rev. A* **57**, 120 (1998); C. H. Bennet and D. P. DiVincenzo, *Nature (London)* **404**, 247 (2000).
- [7] P. Struck and G. Burkard, *Phys. Rev. B* **82**, 125401 (2010).
- [8] M. Gmitra *et al.*, *Phys. Rev. B* **80**, 235431 (2009); A. H. Castro-Neto and F. Guinea, *Phys. Rev. Lett.* **103**, 026804 (2009).
- [9] L. A. Ponomarenko *et al.*, *Science* **320**, 356 (2008).
- [10] C. Stampfer *et al.*, *Appl. Phys. Lett.* **92**, 012102 (2008); F. Molitor *et al.*, *Appl. Phys. Lett.* **94**, 222107 (2009); J. Güttinger *et al.*, *Appl. Phys. Lett.* **93**, 212102 (2008).
- [11] J. Güttinger *et al.*, *Phys. Rev. Lett.* **103**, 046810 (2009); S. Neubeck *et al.*, *Small* **6**, 1469 (2010).
- [12] M. V. Berry and R. J. Mondragon, *Proc. R. Soc. A* **412**, 53 (1987).
- [13] J. Wurm *et al.*, *Phys. Rev. Lett.* **102**, 056856 (2009); F. Libisch, C. Stampfer, and J. Burgdorfer, *Phys. Rev. B* **79**, 115423 (2009).
- [14] J. T. Li *et al.*, *Phys. Rev. Lett.* **80**, 3332 (1998); T. Maltezopoulos *et al.*, *Phys. Rev. Lett.* **91**, 196804 (2003).
- [15] P. Lacovig *et al.*, *Phys. Rev. Lett.* **103**, 166101 (2009).
- [16] I. Pletikosić *et al.*, *Phys. Rev. Lett.* **102**, 056808 (2009).
- [17] K. S. Novoselov and A. K. Geim, *Nature Mater.* **6**, 183 (2007); A. H. Castro Neto *et al.*, *Rev. Mod. Phys.* **81**, 109 (2009); C. Lee *et al.*, *Science* **321**, 385 (2008).
- [18] T. Mashoff, M. Pratzer, and M. Morgenstern, *Rev. Sci. Instrum.* **80**, 053702 (2009).
- [19] A. T. N'Diyae *et al.*, *New J. Phys.* **10**, 043033 (2008); *Phys. Rev. Lett.* **97**, 215501 (2006).
- [20] M. Morgenstern, *Surf. Rev. Lett.* **10**, 933 (2003).
- [21] S. Reich *et al.*, *Phys. Rev. B* **66**, 035412 (2002).

- [22] A. Grüneis *et al.*, *Phys. Rev. B* **78**, 205425 (2008).
- [23] F. Libisch *et al.*, *Phys. Rev. B* **81**, 245411 (2010).
- [24] See Supplemental Material at <http://link.aps.org/supplemental/10.1103/PhysRevLett.108.046801> for STM-images of all graphene QDs studied, additional information about the performed DFT calculation, and further spectroscopic images comparing the graphene confined states with the calculated images as well as images of the standing wave pattern caused by the Ir surface state within and outside the QDs.
- [25] C. Busse *et al.*, *Phys. Rev. Lett.* **107**, 036101 (2011).
- [26] S. Rusponi *et al.*, *Phys. Rev. Lett.* **105**, 246803 (2010).
- [27] A. Varykhalov *et al.*, [arXiv:1104.3308](https://arxiv.org/abs/1104.3308); J. v. d. Veen, F. J. Himpsel, and D. E. Eastman, *Phys. Rev. B* **22**, 4226 (1980).
- [28] P. Giannozzi *et al.*, *J. Phys. Condens. Matter* **21**, 395502 (2009), <http://www.quantum-espresso.org>.
- [29] K. Nakada *et al.*, *Phys. Rev. B* **54**, 17954 (1996).
- [30] C. Wittneven *et al.*, *Phys. Rev. Lett.* **81**, 5616 (1998).
- [31] Plotting $E(\pi/\lambda)$ for standing waves would correspond to plotting the usual $E(2\pi/\lambda)$ for Bloch waves; E. J. Heller *et al.*, *Nature (London)* **369**, 464 (1994).
- [32] S.H. Park *et al.*, *ACS Nano* **5**, 8162 (2011); S.K. Hämäläinen *et al.*, *Phys. Rev. Lett.* **107**, 236803 (2011).